Accepted Manuscript

Solar Energetic Particle Events during the Rise Phases of Solar Cycles 23 and 24

R. Chandra, N. Gopalswamy, P. Mäkelä, H. Xie, S. Yashiro, S. Akiyama, W. Uddin, A.K. Srivastava, N.C. Joshi, R. Jain, A.K. Awasthi, P.K. Manoharan, K. Mahalakshmi, V.C. Dwivedi, D.P. Choudhary, N.V. Nitta

PII: S0273-1177(13)00569-3
DOI: http://dx.doi.org/10.1016/j.asr.2013.09.006
Reference: JASR 11502

To appear in: *Advances in Space Research*

Received Date: 25 November 2012
Revised Date: 3 September 2013
Accepted Date: 5 September 2013

Please cite this article as: Chandra, R., Gopalswamy, N., Mäkelä, P., Xie, H., Yashiro, S., Akiyama, S., Uddin, W., Srivastava, A.K., Joshi, N.C., Jain, R., Awasthi, A.K., Manoharan, P.K., Mahalakshmi, K., Dwivedi, V.C., Choudhary, D.P., Nitta, N.V., Solar Energetic Particle Events during the Rise Phases of Solar Cycles 23 and 24, *Advances in Space Research* (2013), doi: http://dx.doi.org/10.1016/j.asr.2013.09.006

Solar Energetic Particle Events during the Rise Phases of Solar Cycles 23 and 24

R. Chandra
Department of Physics, DSB Campus, Kumaun University, Nainital 263 002, India

N. Gopalswamy, P. Mäkelä, H. Xie, S. Yashiro, and S. Akiyama
NASA Goddard Space Flight Center, Greenbelt, MD 20771-0001, USA

W. Uddin, A. K. Srivastava, and N. C. Joshi
ARIES, Manora Peak, Nainital 263 129, India

R. Jain and A. K. Awasthi
Physical Research Laboratory, Ahmedabad 380 009, India

P. K. Manoharan, K. Mahalakshmi, and V. C. Dwivedi
TIFR/NCRA Radio Astronomy Center, Ooty 643 001, India

D. P. Choudhary
Department of Physics & Astronomy, California State University, Northridge, CA 91330-8268 USA

N. V. Nitta
Lockheed Martin Solar and Astrophysical Laboratory, A021S, Hanover Street, Palo Alto, CA 94304, USA

Abstract: We present a comparative study of the properties of coronal mass ejections (CMEs) and flares associated with the solar energetic particle (SEP) events in the rising phases of solar cycles (SC) 23 (1996-1998) (22 events) and 24 (2009-2011) (20 events), which are associated with type II radio bursts. Based on the SEP intensity, we divided the events into three categories, i.e. weak (intensity <1 pfu), minor (1pfu <intensity <10 pfu) and major (intensity ≥ 10 pfu) events. We used the GOES data for the minor and major SEP events and SOHO/ERNE data for the weak SEP event. We examine the correlation of SEP intensity with flare size and CME properties. We find that most of the major SEP events are associated with halo or partial halo CMEs originating close to the sun center and western-hemisphere. The fraction of halo CMEs in SC 24 is larger than the SC 23. For the minor SEP events one event in SC23 and one event in SC24 have widths < 120^o and all other events are associated with halo or partial halo CMEs as in the case of major SEP events. In case of weak SEP events, majority (more than 60 %) of events are associated with CME width < 120^o. For both the SC the average CMEs speeds are similar. For major SEP events, average CME speeds are higher in comparison to minor and weak events. The SEP event intensity and GOES X-ray flare size are poorly correlated. During the rise phase of solar cycle 23 and 24, we find north-south asymmetry in the SEP event source locations: in cycle 23 most sources are located in the south, whereas during cycle 24 most sources are located in

the north. **This result is consistent with the asymmetry found with sunspot area and intense flares.**

Keywords: *Solar Energetic particles, Type II radio bursts, Coronal Mass Ejections, Flares*

Corresponding author: R. Chandra, rchandra.ntl@gmail.com (ph: +91-5942-237450, fax: +91-5942-237450)

1. Introduction

One of the most important and interesting aspects of a solar eruption is the acceleration of solar energetic particles (SEPs). It is believed that SEPs are accelerated at the shock ahead of coronal mass ejections (CMEs) (Kahler et al. 1978) or at the magnetic reconnection regions associated with solar flares (Mason et al. 1999). SEP events due to CME-driven shocks are large and gradual (long duration) in nature (Reames, 1999). Solar type -II radio bursts are also due to shocks from a solar eruption. Therefore, observations of type II bursts give information on shock associated SEPs. On the contrary, SEP events produced by the flare reconnection process are impulsive and short-lived in nature (Cane et al. 1986; Reames, 1999; Laurenza et al. 2009; Cane et al. 2006; Bhatt et al. 2013). Both the shock and flare are expected to occur during energetic solar eruptions. Therefore, it might be possible that the observed SEPs are due to the combined effects of these two processes. However, there are examples in the literature where there was SEP event but no type II radio burst (Gopalswamy et al. 2004). Such events can be safely attributed solely to flare acceleration, happening low in the corona. CMEs associated with SEPs generally originate from solar active regions (Gopalswamy et al. 2010a). However, there are examples of CMEs associated with quiescent filament eruption (Kahler et al. 1986; Vršnak et al. 2003; Titov et al. 2012**; Schmieder and Aulanier 2012**). Active regions can store and release vast amounts of magnetic energy. Due to the enhanced solar activity during the solar maximum phase, most of the SEP events occur in this phase, which makes it difficult sometimes to identify the source region of CMEs (for example Chandra et al. 2010). In the rise phase of the solar cycle, SEP events are less frequent, thus providing a better opportunity to study the SEP events including the detection of their source region.

If the CMEs are faster, they drive stronger shocks, so there should be good correlation between CME speed and SEP events intensity. Many studies have shown good correlation between the SEP intensity and CME speed, but the correlation is not tight. On the other hand, the correlation between SEPs intensity and flare size is generally poor (Gopalswamy et al. 2003, 2004). Gopalswamy et al. (2004) found that SEP events preceded by wide CMEs from the same source region within 24 hour are associated with intense SEP events.

Recently Miteva et al. (2013) studied SEP events associated with GOES X- and M-class flares originating from the western hemisphere and found different correlation between CME speed and SEP intensity depending upon the interplanetary magnetic field (IMF) configuration into which the SEPs propagate. The IMF configuration seems to be another parameter that can introduce variability in SEPs.

Gopalswamy (2012) compared solar activity during SC 23 and 24 on the space weather events such as large SEPs and major geomagnetic storms. He concluded that the number of large SEP events of SC 24 is similar to that in the corresponding epoch of SC 23. The CMEs associated with large SEPs are very energetic; however, they appear to be less efficient in accelerating particles. Keeping the above results in mind, we would like to explore if these results are also applicable to weaker SEP events.

In this paper, we present a comparative study of SEP events, CMEs, flares, and their correlations during the rise phase of solar cycles (SC) 23 and 24. Such a study was recently performed, but considering only large SEP events (Gopalswamy 2012). We extend our study to weaker SEP events. The paper is organized as follows: The data selection is described in section 2; Section 3 presents the properties of SEP events and the associated phenomena. Finally, in section 4 summarize our study.

2. Data Sets

For the current study, we have selected SEP events, which are associated with metric type II radio bursts. There is a high degree of association between SEP events and metric type II radio bursts. This association can be explained as follows: CMEs drive the shock, which accelerates electrons and ions. The accelerated electrons produce type II bursts and the protons are observed as SEPs.

We divided the SEP events into three categories, viz., weak (proton intensity < 1 pfu, 1 pfu = 1 proton cm^{-1} s^{-1} sr^{-1}), minor (1 pfu $\leq$ proton intensity <10 pfu) and major (proton intensity$\geq$ 10 pfu), respectively. With this criterion, we have more number of events than in Gopalswamy (2012b), who considered only $\geq$ 10 pfu events.

We have used SEP events data from GOES in the >10 MeV energy channel for the minor and major events. The weak SEP events are not clearly distinguishable in GOES data. Therefore for weak SEP events, we have used the data from the Energetic and Relativistic Nuclei and Electron (ERNE, Torsti et al. 1995) instruments onboard SOHO in 12.6 – 140 MeV energy range. The ERNE data has high sensitivity; hence it is useful to detect the weaker SEP events. The proton flux in ERNE data is in proton cm^{-1} s^{-1} sr^{-1}/n (pfu/n), whereas the GOES data is in pfu unit. For the consistency, we have converted the ERNE data into pfu unit by multiplying the channel width. The temporal resolution of ERNE data is 5 min. An example of the comparison between the GOES and ERNE proton flux on 07 – 08 August, 2010 is plotted in figure 2 (bottom panel). The figure indicates very good consistency in the GOES and ERNE data.

The GOES data are available at http://sec.noaa.gov, while the SOHO/ERNE data are downloaded from http://www.srl.utu.fi/erne_data/datafinder/df.shtml. CME data are from the Large Angle and Spectrometric Coronagraph (LASCO, Brueckner et al. 1995) onboard SOHO as cataloged at the CDAW Data Center (http://cdaw.gsfc.nasa.gov, Gopalswamy et al. 2009). The LASCO C2 and C3 telescopes obtain images of the corona from ~ 2 to 32 Rs field of view (FOV). The CMEs source location on the solar disk was searched using available images, movies and Solar Geophysical data (SGD) list: for example movies from SOHO/EIT, movies from Yohkoh/SXT. For solar cycle 24, we also included the high spatial and temporal resolution movies from the Solar Dynamic Observatory (SDO). For the X-ray and optical classification, we used the event lists from the SGD. The metric type II burst data obtained by various ground based instruments are available online (ftp://ftp.ngdc.noaa.gov/STP/SOLAR_DATA/SOLAR_RADIO/SPECTRAL/).

The selected events are listed in Table I and II for the rising phase of SCs 23 (1996 – 1998) and 24 (2009 - 2011), respectively. The data analysis involves examining plots and CMEs associated with metric type II radio bursts. Figure 1 shows one of the examples of a largest SEP event in the rise phase of SC 23 and its solar source region. The CME source region is on the west limb (S43W90). The CME was very fast (1863 km/s) and wide (>243^{o}). The event was associated with an M-class flare. Information like this are listed in Tables I and II for all the events considered in this paper.

3.0 Results and Discussion

In this section, we describe the properties of SEPs, associated CMEs, flares and their source locations. Looking at tables I and II, we see that the number of SEP events in the rise phase of both the cycles is nearly the same (22 in SC23 and 20 in SC24). However, the rise phase of SC 24 is weaker than that of SC 23. The detailed description is presented in following subsections.

3.1 SEP Intensities

We have plotted the proton intensities and the number of SEP events during the rise phases of SCs 23 and 24 in figure 3. The average values in SC23 and 24 are 115 and 10 pfu, whereas the median values are 1 and 3 pfu, respectively. The median intensities are similar in both cases, but the mean intensity is much higher for SC 23 because there were four high-intensity events during the rise phase of SC 23 (see also Gopalswamy 2012b). We think that the high intensity events in SC 23 are indicative of the higher level of solar activity in that cycle compared to SC24. In other words there is an overall reduction in the number of severe space weather events during SC24. The correlation between intensities and number of SEP events is significant and it is higher for large events (Gopalswamy et al. 2004). We extend here it for weaker SEP events.

3.2 CME Characteristics

It is generally known that western fast and wide CMEs are strong producers of SEP events at Earth. In Miteva et al. (2013) classification, they find the CMEs having width >60^o have strong correlation in comparison to all events

Figure 4 shows the distribution of speed, width, and source longitude of CMEs associated with SEP events. We see that the average (~900 km/s) and median (~800 km/s) speeds of the SEP-producing CMEs are in the same range during the two cycles. Comparing the widths of CMEs associated with SEPs in SCs 23 and 24, we find that most of the CMEs are wide (width at least 60^0, except three events in SC24). The average and median widths, respectively are 140^0, 143^0 (SC23) and 122^0, 125^0 (SC24), which confirm the earlier studies that wider CMEs are more capable of producing stronger SEP events. The last bin in the width distributions corresponds to halo CMEs. Halo CMEs are more energetic compared to normal CMEs (Gopalswamy et al. 2010b). The fraction of halo CMEs in the CME populations of SC23 and 24 that produced SEPs are 36% and 50%, respectively. Clearly, the fraction of halo CMEs is larger during SC 24. The fraction is almost 100% when only large SEP events are considered (Gopalswamy 2012b).

We identified the source regions of CMEs using various data sets mentioned in section 2. The source longitudes are plotted in the bottom panel of figure 4. It is clear that almost all the sources are located in the western hemisphere (except three sources in SC 23 and one source in SC 24). The results are consistent with the fact that western active regions produce strong SEP events at Earth, as it was reported in previous studies (Gopalswamy et al. 2008; Manoharan and Agalya 2011) because those active regions are magnetically well-connected to Earth.

Since SEPs are accelerated by CME-driven shocks, the SEP intensity is correlated with CME speed (Kahler, 2001, Gopalswamy et al. 2003; 2004 and references therein). The CME speed - proton intensity plot in figure 5 for the rise phases of SC 23 and SC24 shows only a weak correlation (R ~ 0.45). The correlation coefficients are in the same range for both the solar cycles. This indicates that the CME speed alone is not responsible for strong SEP events. Gopalswamy et al. (2004) and Gopalswamy (2012a) introduced a few possibilities for higher SEP intensities, such as interaction of two or more CMEs and CME interaction with coronal holes.

In figure 4, we see that some low speed CMEs are associated with SEP events. This can be explained as follows: first, we have not corrected for projection effects, so the measured LASCO CME speeds may be underestimated. Another possibility may be that the coronal environment played a role. Gopalswamy et al. (2008a, b) concluded that either some fast and wide CMEs do not drive shocks or if they do the shocks may be too weak to produce SEP event. They have also concluded that the Alfven speed in the corona and near-Sun inter-planetary medium varies from < 200 km/s to ~1600 km/s. Therefore, if the Alfven speed is low, even slow CMEs can be associated with SEPs. On the other hand if the Alfven speed is high, even high speed CMEs may not be associated with SEPs. In the case of very high CME speeds (> 2000 km/s), the Alfven speed may not play an important role because the CMEs will always be super-Alfvenic and hence they produce SEP events at Earth, provided the source region is located in the western hemisphere.

3.3 Flare Characteristics

In this section, we compare the X-ray flare sizes for the SEP events during SC23 and SC24. For the flare size, we use the peak soft X-ray flux (in units of W m^{-2}) in the GOES 1-8 Å channel. The results are shown in figure 6. In the rise phase of SC23, out of 22 SEPs, 6 were associated with X-class flare, 8 with M-class, 5 with C-class, and 1 with B-class flares; one event was associated with a quiescent prominence eruption (see figure 1). In the rise phase of SC24, out of 20 SEPs, 2 were associated with X-class flare, 12 with M-class, 5 with C-class, and 1 with B-class flares. From this analysis we see that a majority (66%) of SEPs was associated with X or M class flares. There is no major difference in the flare sizes between the two cycles. In figure 7, we have plotted the GOES X-ray peak flux against the proton intensity. The X-ray peak flux and proton intensity are very poorly correlated as reported in previous observations (Gopalswamy et al. 2003; 2004). The correlation coefficients in SC 23 and 24 are 0.18 and 0.19 respectively.

We also compiled various properties of CMEs for the major, minor, and weak SEPs in Table III. The average CME speed associated with major SEPs for SC23 and 24 are 1241 and 1320 km/s, respectively. For minor and weak SEPs the average CME speeds are 975 (774) and 536 (539) km/s for the SC23 (24), respectively. We do not find any significant difference in CME speeds between the two cycles. For the major SEP events the fraction of halo CMEs is much larger in SC24 (83%) than in SC23 (57 %). In the case of minor SEP events the fraction is similar. For weak SEP events there is no halo CME in SC23 whereas there is only one halo CME in SC24. For the major SEP events all CMEs are halos or partial halos ($\geq 120^{o}$). CMEs with width $<120^{o}$ can be found only for weak SEP events.

In a similar study involving major SEP events for the whole of solar cycle 23 Gopalswamy et al. (2004) found the average and median speeds of SEP-associated CMEs are 1468 km/s and 1369 km/s respectively. Our results for major SEP events are consistent with Gopalswamy et al. (2004) results.

Gopalswamy (2012), studied the SEP events during rise phase of SC23 and 24 having intensity > 10 pfu in >10 MeV energy channel using GOES data and found the following results: (1) the average

Speed of the SEP-associated CMEs during SC 23 & 24 is 1373 km/s and 1651 km/s respectively. (2) 95 % of SEP-associated CMEs are full halos during rise phase of SC 24, whiles 68% are full halos in corresponding epoch of SC 23. (3) SC 24 CMEs are less efficient in accelerating energetic particles in comparison to SC23. Comprising our results with Gopalswamy (2012) results, we found: average CME speed for major SEP events are 1241 km/s and 1320 km/s for SC23 and 24 respectively, which are comparable to Gopalswamy (2012) for SC23 and lower in case of SC24. For the minor and weak SEP events the average CME speeds are very low comparative to major SEP events. The percentage of full halos in case of major event is closer, whiles in case of minor and weak SEP events the percentage of halo CMEs is very low in comparisons to Gopalswamy (2012). The above comparison indicate that our present study confirms the results of Gopalswamy (2012b) for the SEP events > 10 pfu and give different results in case of minor and weak SEP events.

3.2 **Asymmetry during solar cycle 23 and 24**

It is well known that different solar activity features (such as solar flares, filaments, magnetic flux, and relative sunspot numbers) exhibit north-south asymmetry.

There are several studies that deal with the asymmetry of different solar activity feature using the data of soft X-rays, sunspots numbers and H-alpha flares (Li et al. 2009; Joshi and Joshi 2004; Verma, 1993). Asymmetry has been also reported in the interplanetary magnetic field (IMF) observations (Ebert et al. 2013; Wang and Sheeley, 2013; Manoharan 2012).To understand the asymmetry behavior of solar cycle, our study give the another parameter i.e. source location of the SEPs.

North-South asymmetry in soft X-ray flare occurrence was studied by Garcia et al. (1990) (SC 20, 21) and Joshi and Joshi (2004) (SC21, 22 and 23). The rise phase activity in SC24 is similar to that in SC20 and SC21 but opposite to that in SC 23. Our results in the rise phase of SC24 are consistent with Joshi et al. (2008) results of SC22. The asymmetry study of the sunspot area during the SC23 revealed that during the rise phase of SC23 the activity is southern dominated, which is consistence with SEP event results for SC23 (Li et al. 2009). This consistency arises from the fact that SEP events originate in active regions that have large sunspots, and produce intense flares (Gopalswamy et al. 2010b).

To see this behavior in SEP events solar sources, we have plotted the location of SEP source region in the rise phases of SC 23 and 24 in figure 8. We see that the SC 23 source regions are mostly in the southern hemisphere (nineteen sources in south and three sources in north). On the contrary, the SC 24 sources are mostly in the northern hemisphere (seventeen sources in north and three sources in south). This indicates a clear north-south asymmetry in the rising phases of SC 23 and SC 24. In SC 23 the activity begins in northern hemisphere. However, in SC 24 the activity started in the southern hemisphere. This indicates the delay between the activity in northern and southern hemisphere as was shown by Gopalswamy (2012b) for large SEP events.

4. Summary

In this study, we compared SEP events and the associated phenomena (such as CME speed, width, and longitude), flare size, source location during the rise phases of solar cycles 23 and 24. We summarize our main results as follows:

- In the rise phase of solar cycle 23 the SEP events are stronger than those of solar cycle 24.
- The distribution of source region of SEPs shows north-south asymmetry. In the rise phase of solar cycle 23 the SEPs source regions are mostly in the southern hemisphere. On the contrary, the SEPs source regions are mostly in the northern hemisphere during the rise phase of cycle 24.
- We find a correlation coefficient of ~ 0.45 between the CME speed and proton flux, but it is not tight. This correlation indicates there are other variable that determine the strength of SEPs.
- There correlation between the X-ray flare size and SEPs intensity is rather poor, which confirms earlier results.
- Our study extends the earlier study of Gopalswamy (2012) for the weaker SEP events (< 10 pfu).

Acknowledgments: The authors thank the anonymous referee's for their comments and suggestions, which improve the paper considerably. This study was conducted as a part of the Indo-US Science and Technology Forum's Joint Center on Solar Eruptive events. We acknowledge the open data policy of NGDC, ERNE, SOHO and SDO. RC, WU and AKS also acknowledge the partial support from ISRO/RESPOND project no. ISRO/RES/2/379/12-13.

References

Bhatt, N. J., Jain, R. Awasthi, A. K. Energetic relationship among geoeffective solar flares, associated CMEs and SEPs. Res. Astronomy and Astrophysics 13, 978-990, 2013.

Brueckner, G. E., Howard, R. A., Koomen, D. J., et al. The Large angle spectroscopic coronagraph (LASCO). Solar Phys. 162, 357-402, 1995.

Cane, H. V., Mewaldt, R. A., Cohen, C. M. S., von Rosenvinge, T. T. Role of flares and shocks in determining solar energetic particle abundance. J. Geophys. Res. 111, A06590, doi: 10.1029/2005JA011071, 2006.

Cane, H. V., McGuire, R. E., von Rosenvinge, T. T. Two classes of solar energetic particle events associated with impulsive and long-duration soft X-ray flares. Astrophys. J. 301, 448-459, 1986.

Chandra, R., Pariat, E., Schmieder, B., Mandrini, C. H., Uddin, W. How can a negative magnetic helicity active region generate a positive helicity magnetic cloud ? Sol. Phys. 261, 127-148, 2010.

Ebert, R. W., Dayeh, M. A., Desai, M. I., McComas, D. J., Pogorelov, N. V. Hemispheric asymmetries in the polar solar wind observed by Ulysses near the minima of solar cycles 22 and 23. Astrophys. J. 768, 160-170, 2013.

Garcia, H. A. Evidence of solar-cycle evolution of north-south flare asymmetry during cycles 20 and 21. Sol. Phys. 127, 185-197, 1990.

Gopalswamy, N., Yashiro, S., Lara, A., Kaiser, M. L., Thompson, B. J., Gallagher, P. T., Howard, R. A. Large solar energetic particle events of cycle 23: A global view. J. Geophys. Res. Lett. 30, doi: 10.1029/2002GL016435, 2003.

Gopalswamy, N., Yashiro, S., Krucker, S., Stenborg, G., Howard, R. A. Intensity variation of large solar energetic particle events associated with coronal mass ejections. J. Geophys. Res. 109, A12015, doi: 10.1029/2004JA010602, 2004.

Gopalswamy, N., Yashiro, S., Akiyama, S., Mäkelä, P., Xie, H., Kaiser, M. L., Howard, R. A., Bougeret, J. L. Coronal mass ejections, type II radio bursts, and solar energetic particle events in the SOHO era. Ann. Geophys. 26, 3033-3047, 2008a.

Gopalswamy, N., Yashiro, S., Xie, H. et al. Radio-quiet fast and wide coronal mass ejections. Astrophys. J. 674, 560-569, 2008b.

Gopalswamy, N., Yashiro, S., Michalek, G., Stenborg, G., Vourlidas, A., Freeland, S., Howard, R. The SOHO/LASCO CME Catalog. Earth, Moon, and Planets.104, 295-313, 2009.

Gopalswamy, B., Akiyama, S., Yashiro, S., and Mäkelä, P. Coronal mass ejections from sunspot and non-sunspot regions. in S.S. Hasan and R.J. Rutten (eds.), Magnetic Coupling between the Interior and Atmosphere of the Sun, Springer, pp. 289-307, 2010a.

Gopalswamy, N., Yashiro, S., Michalek, G., Xie, H., Mäkelä, P., Vourlidas, A., Howard, R. A. A Catalog of Halo Coronal Mass Ejections from SOHO. Sun and Geosphere. 5(1), 7-16, 2010b.

Gopalswamy, N. Factors Affecting The Intensity of Solar Energetic Particle Events, in Proc. Tenth annual Astrophysics Conf., ed. J. Heerikhuisen, G. Li, and G. Zank, American Institute of Physics, pp. 247-252, 2012a.

Gopalswamy, N. Energetic particle and other space weather events of solar cycle 24. in Proc. 11th Annual Astrophysical Conference, AIP conference proceedings, 1500, pp. 14-19, 2012b.

Joshi, B., Joshi, A. The north-south asymmetry of soft x-ray flare index during solar cycles 21, 22 and 23. Sol. Phys. 261, 343-356, 2004.

Kahler, S. W., Cliver, E. W., Cane, H. V., McGuire, R. E., Stone, R. G., Sheeley, N. R. Solar filament eruptions and energetic particle events. Astrophys. J. 302, 504-510, 1986.

Kahler, S. W., Hildner, E., Van Hollebeke, M. A. I. Prompt solar proton events and coronal mass ejections. Sol. Phys. 57, 429-443, 1978.

Kahler, S. W. The correlation between solar energetic particle peak intensities and speeds of coronal mass ejections: Effects of ambient particle intensities and energy spectra. J. Geophys. Res. 106, 20947-20956, 2001.

Laurenza, M., Cliver, E. W., Hewitt, J., et al. A technique for short-term warning of solar energetic particle events based on flare location, flare size, and evidence of particle escape. Space Weather. 7, S04008, doi: 10.1029/2007SW000379, 2009.

Li, K. J., Gao, P.X., Zhan, L.S. The Long-term behaviour of the north-south asymmetry of sunspot activity. Sol. Phys. 254, 145-154, 2009.

Manoharan, P. K. Three-dimensional evolution of solar wind during solar cycles 22-24. Astrophys. J. 751, 128-141, 2012.

Manoharan, P. K. , Agalya, G. High energy solar particle events and their associated coronal mass ejections. Advances in Geosciences, Solar Terrestrial (ST). Edited by Marc Duldig, Singapore: World Scientific, 27, pp.165-179, 2011.

Mason, G. M., Mazur, J. E., Dwyer, J. R. ^{3}He enhancements in large solar energetic particle events. Astrophys. J. 525, L133-L136, 1999.

Miteva, R., Klein, K.-L., Malandraki, O., Dorrian, G. Solar energetic particle events in the 23rd solar cycle: Interplanetary magnetic field configuration and statistical relationship with flares and CMEs. Sol. Phys. 282, 579-613, 2013.

Reames, D. V. Particle acceleration at the Sun and in the heliosphere. Space Science Reviews. 90, 413-491, 1999.

Schmieder, B. and Aulanier, G. What are the physical mechanism of eruptions and CMEs ? Adv. Space. Res. 49, 1598-1606, 2012.

Titov, V. S., Mikic, Z., Török, T., Linker, J. A., Panasenco, O. 2010 August 1-2 Sympathetic Eruptions. I. Magnetic topology of the source-surface background field. Astrophys. J., 759, 70-87, 2012.

Torsti, J., Valtonen, E., Lumme, M., et al. Energetic particle experiment ERNE. Sol. Phys. 162, 505-531, 1995.

Verma, V. K. On the north-south asymmetry of solar active cycles. Astrophys. J. 403, 797-800, 1993.

Vršnak, B., Warmuth, A.,Maričić, D., Otruba, W., Ruždjak, V. Interaction of an erupting filament with the ambient magnetoplasma and escape of electron beams. Sol. Phys. 217, 187-198, 2003.

Wang, Y.-M., Sheeley, N. R., Jr. The solar wind and interplanetary field during very low amplitude sunspot cycles. Astrophys. J. 764, 90-100, 2013.

Figure Captions:

Figure 1: An example of major SEP event and its source region on 20 April, 1998: Three snapshots of the CME that produced the SEP event (top panel), the time variation of SEP intensity in three energy channels (>10 MeV, > 50 MeV, and > 100 MeV) (upper middle panel), the CME height-time plot of the CME (lower middle panel), the soft X-ray flare light curves in the two energy channels (bottom panel).

Figure2: An example of weak SEP event on 7-8 August, 2010 observed by GOES and SOHO/ERNE. Top panels represent the dynamic radio spectra observed by RSTN and WAVES/WIND, and lower panel represent the comparison of SEP events observed by GOES and SOHO/ERNE instruments.

Figure3: Distribution of proton intensity with number of events during the rising phase of solar cycle 23 (left) and 24 (right), respectively.

Figure 4: Properties of CMEs associated with SEPs: Speed (top panel), Width (middle panel), and Location of the CME source region (bottom panel), respectively during the rising phase of solar cycle 23 (left) and 24 (right).

Figure 5: Scatter plots between CME speed and proton intensity for the rising phases of solar cycle 23 (left) and 24 (right) respectively. The regression line and correlation coefficients (R) are also shown in the figure.

Figure6: Distribution of GOES X-ray peak flux with number of events during the rising phase of solar cycle 23 (left) and 24 (right) respectively.

Figure 7: The scatter plots between X-ray peak flux and proton intensity for the rising phase of solar cycle 23 (left) and 24 (right) respectively. The regression line is also shown for each group. The correlation coefficients (R) are also indicated.

Figure 8: Distribution of SEPs source region during the rise phases of solar cycle 23 (black circle) and 24 (red triangle), respectively.

Table I: SEPs in the rise phase of solar cycle 23

S.N.	Date	Type II time	SEP time	CME time	CME speed	CME width	location	proton flux (pfu)	AR	flare imp	flare onset
1	960709	09:11	10:22	12:28	452	86	S10W30	0.1 (w)	7978	X2.6/1B	09:01
2	961224	13:09	14:47	13:28	325	69	>W90	0.1 (w)	-	C2.1/?	13:03
3	970407	13:58	16:14	14:27	878	H	S30E19	1 (m)	8027	C6.8/3N	15:50
4	979512	04:54	07:13	05:30	464	H	N21W19	1(m)	8038	C1.3/?	04:42
5	970725	20:24	22:28	21:01	611	84	N17W52	0.3(w)	8065	C2.0/SF	20:00
6	970924	02:48	03:14	03:38	532	76	S31E15	0.3(w)	8088	M5.9/1B	02:43
7	971007	12:48	13:50	13:30	1271	167	>W90	0.5 (w)	No AR	?	?
8	971103	09:08	11:29	11:11	352	122	S20W15	0.2(w)	8100	M1.4/1B	09:03
9	971103	10:26	11:29	11:11	352	122	S20W15	0.2(w)	8100	M4.2/?	10:18
10	971104	05:58	07:00	06:10	785	H	S17W32	72 (M)	8100	X2.1/2B	05:52
11	971106	11:53	13:05	12:10	1556	H	S18W63	490(M)	8100	X9.4/2B	11:49
12	971114	01:31	00:00	22:25*	456	288	N30W65	1(m)	8106	B-class	---
13	980126	22:27	23:55	23:27	399	66	S17W55	0.1(w)	8142	C5.4/SN	22:19
14	980420	09:56	11:00	10:07	1863	165	S43W90	1700(M)	PE	M1.4/?	09:38
15	980429	16:22	00:00*	16:38	1374	H	S18E20	1(m)	8210	M6.8/?	16:06
16	980502	13:41	14:00	14:06	938	H	S15W15	150(M)	8210	X1.1/3B	13:31
17	980506	08:03	08:00	08:29	1099	190	S11W65	210(M)	8210	X2.7/1N	07:58
18	980508	02:00	03:49	02:28	371	76	>W90	1(m)	-	M3.1/?	01:49
19	980509	03:26	05:00	03:35	2331	178	>SW90	12 (M)	8210	M7.7/?	03:04
20	980616	18:18	20:00	18:27	1484	281	S20W90	1(m)	-	M1.0/?	18:03
21	981105	19:50	00:00*	20:44	118	H	N22W18	10(M)	8375	M8.4/?	19:00
22	981124	02:17	03:52	02:30	1798	H	>W90	1(m)	No AR	X1.0/?	02:27

*time corresponds to next day; PE: Prominence Eruption; Proton intensity < 1 pfu (weak, w); 1 pfu ≤ proton intensity <10 pfu (minor, m); proton intensity ≥ 10 pfu (major, M).

Table II: SEPs in the rise phase of solar cycle 24

S.N.	Date	Type II Time	SEP Time	CME			Location	Proton flux (pfu)	AR	flare imp	flare onset
				time	speed	width					
1	100612	00:57	03:30	01:31	486	119	N23W43	0.5 (w)	11081	M2.0/SN	00:30
2	100807	18:08	20:22	18:36	871	H	N11E34	0.5 (w)	11093	M1.0/?	17:55
3	100814	09:47	12:30	10:12	1205	H	N14W54	14(M)	11093	C4.4/SF	09:38
4	100818	05:51	06:45	05:48	1471	184	N14W90	4.1(m)	11093	C4.5/?	04:45
5	101231	04:23	05:49	05:00	363	45	N12W57	0.1(w)	11138	C1.5/?	04:00
6	110128	01:01	01:00	01:25	606	119	N13W93	2.8(m)	11149	M1.3/?	00:44
7	110215	01:51	03:00	02:24	669	H	S20W12	2.5(m)	11158	X2.2/?	01:44
8	110307	19:50	21:50	20:00	2125	H	N30W47	12(M)	11164	M3.7/?	19:43
9	110511	02:27	03:50	02:48	745	225	N18W52	0.3(w)	No AR	B8.1/?	02:23
10	110607	06:25	08:20	06:49	1255	H	S21W54	73(M)	11226	M2.5/2N	06:16
11	110802	06:08	07:00	06:36	712	268	N14W15	4(m)	11261	M1.4/?	05:19
12	110803	13:41	14:42	14:00	610	H	N17W30	1(m)	11261	M6.0/?	13:17
13	110804	03:54	05:16	04:12	1315	H	N19W36	60(M)	11261	M9.3/3B	03:41
14	110808	18:03	19:05	18:12	1343	237	N16W61	4(m)	11263	M3.5/1B	18:00
15	110809	08:01	08:45	08:12	1610	H	N17W69	26(M)	11263	X6.9/2B	07:48
16	110904	04:42	05:30	05:12	262	53	N19W67	0.3(w)	11286	C9.0/SF	04:36
17	110906	01:46	02:30	02:24	782	H	N14W07	1(m)	11283	M5.3/1B	01:35
18	110906	?	00:00*	23:05	575	H	N14W18	9(m)	11283	X2.1/?	22:12
19	111119	01:29	07:40	01:45	507	57	N17W71	0.1(w)	11387	C1.0/?	01:21
20	111225	18:20	20:00	18:48	366	125	S22W26	35(M)	11387	M4.0/1N	18:11

*the time corresponds to next day; PE: Prominence Eruption; Proton intensity < 1 pfu (weak, w); 1 pfu ≤ proton intensity <10 pfu (minor, m); proton intensity ≥ 10 pfu (major, M)

Table III - Summary of Results

Property	Major		Minor		Weak	
	SC23	SC24	SC23	SC24	SC23	SC24
No. of SEPs	7	6	7	8	8	6
Average CME speed	1241 km/s	1320 km/s	975 km/s	774 km/s	536 km/s	539 km/s
No. of halos	4 (57.1%)	5 (83.3%)	4 (57%)	4 (50%)	0 (0%)	1(16.6%)
Width $\geq 120^{o}$	3 (42.9%)	1 (16.7%)	2(28.5%)	3 (37.5%)	3(37.5%)	1 (16.6%)
Width $<120^{o}$	0 (0%)	0 (0%)	1 (14.5%)	1 (12.5%)	5(62.5%)	4 (66.8%)

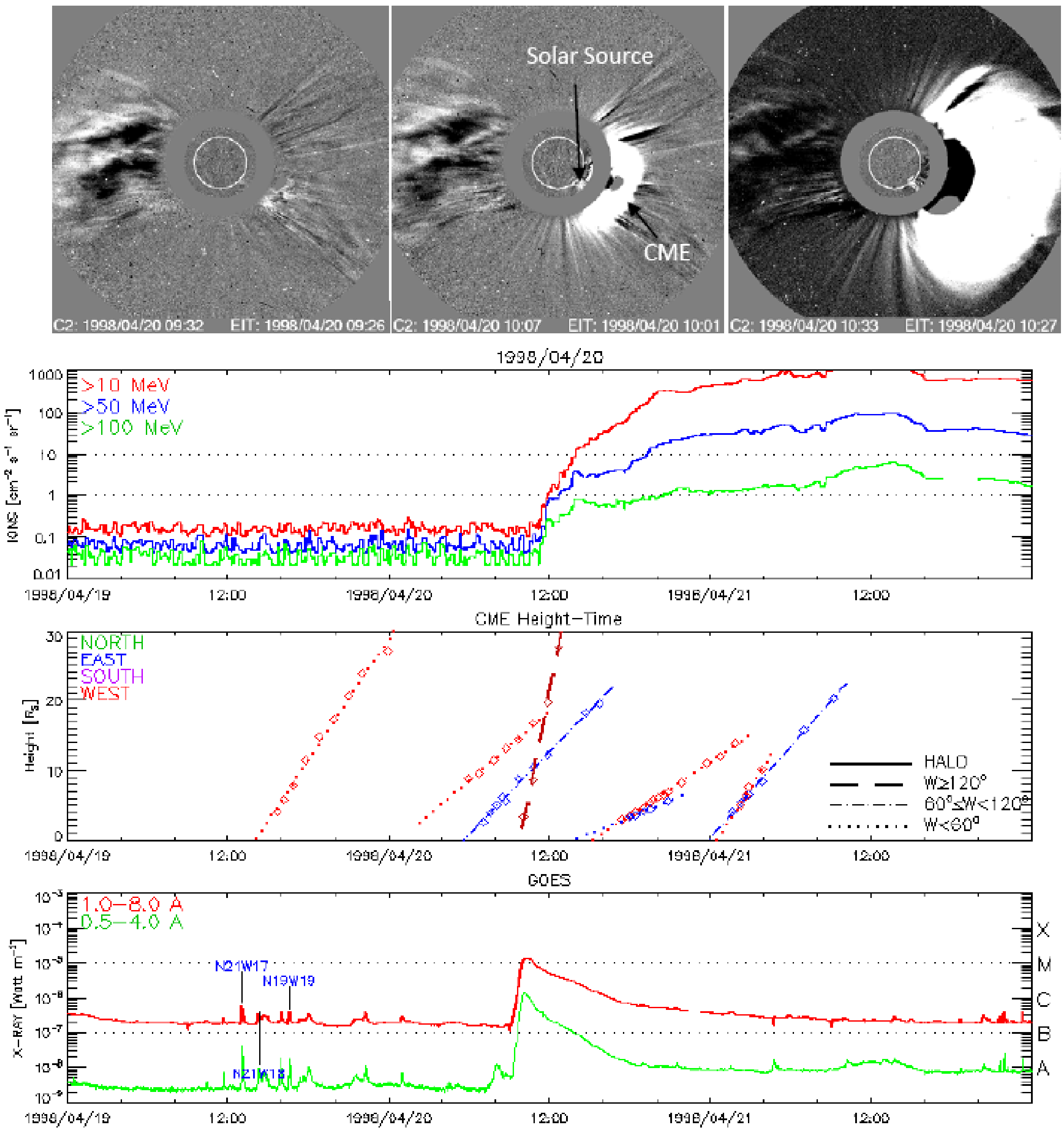

Figure 1: An example of major SEP event and its source region on 20 April, 1998: Three snapshots of the CME that produced the SEP event (top panel), the time variation of SEP intensity in three energy channels (upper middle panel), the CME height-time plot of the CME (lower middle panel), the soft X-ray flare light curves in the two energy channels (bottom panel).

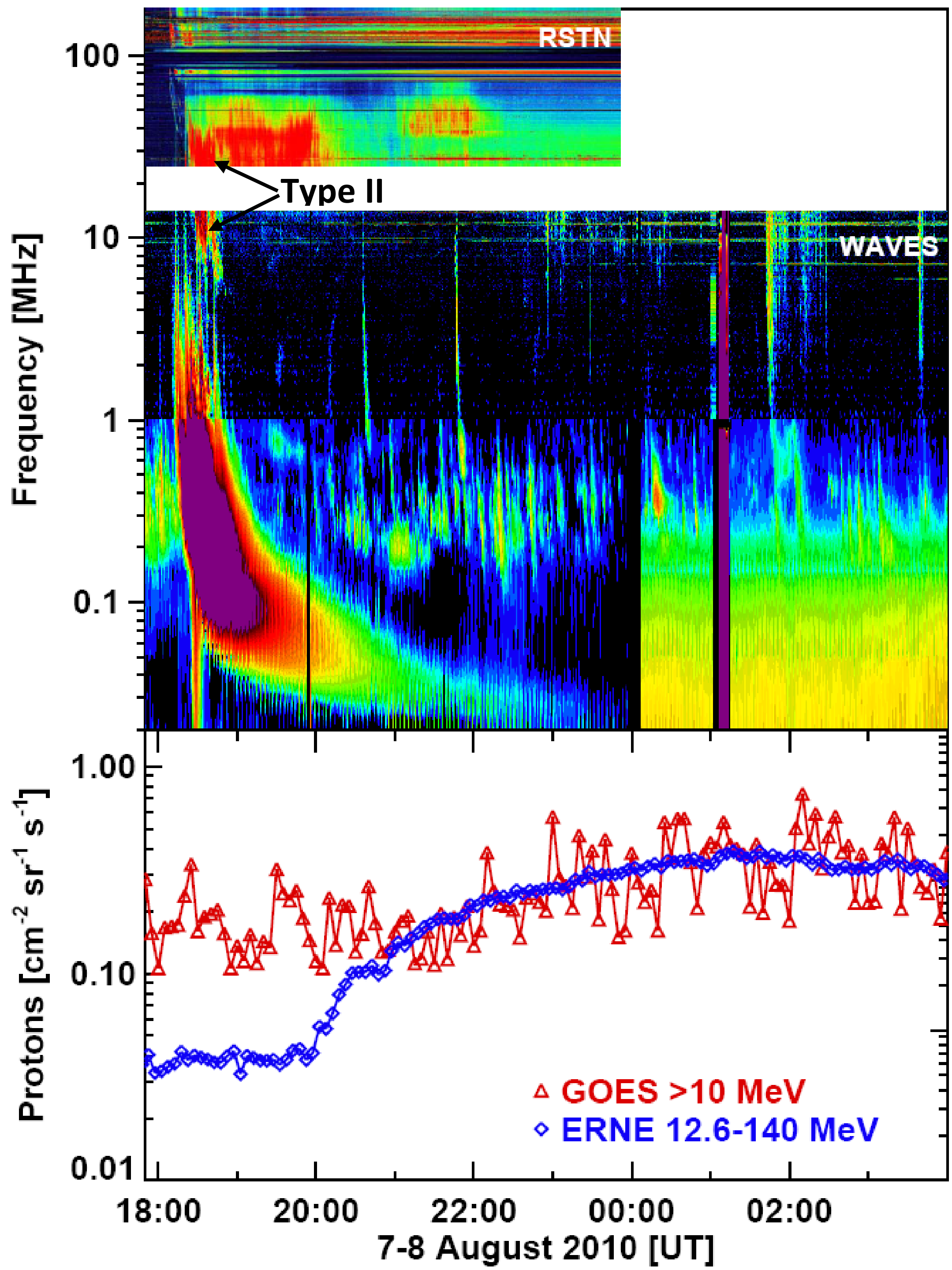

Figure 2: An example of weak SEP event on 7-8 August, 2010 observed by GOES and SOHO/ERNE. Top panels represent the dynamic radio spectra observed by RSTN and WAVES/WIND, and lower panel represent the comparison of SEP events observed by GOES and SOHO/ERNE instruments.

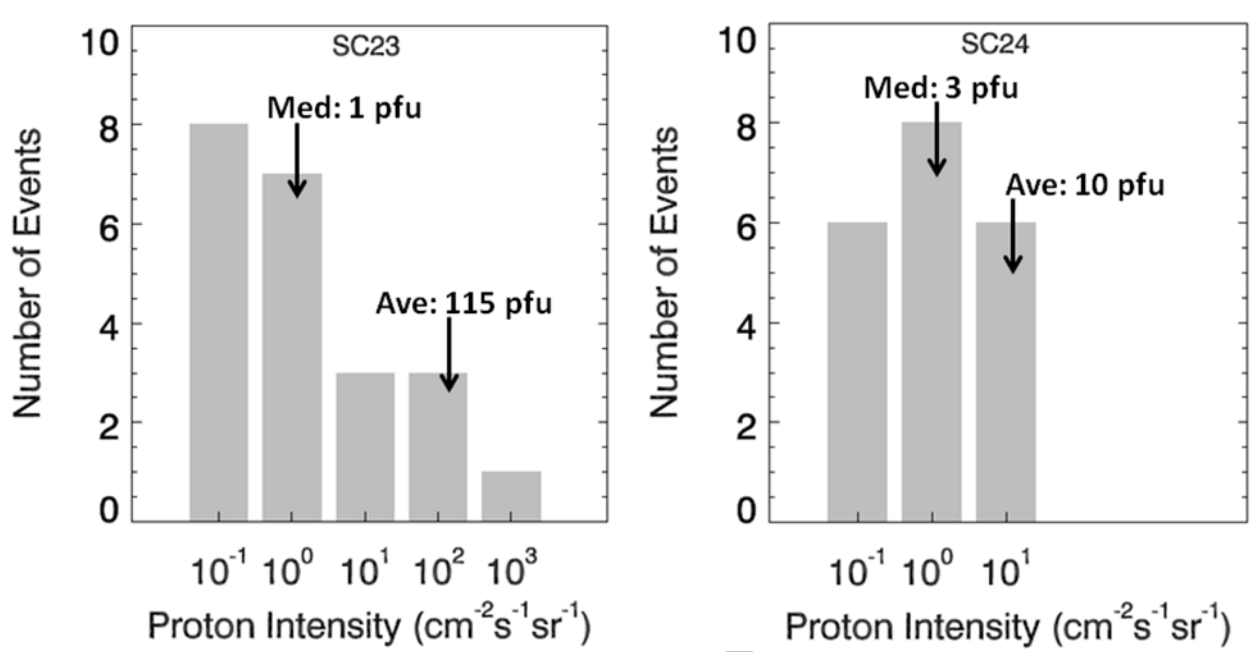

Figure 3: Distribution of proton intensity with number of events during the rising phase of solar cycle 23 (left) and 24 (right).

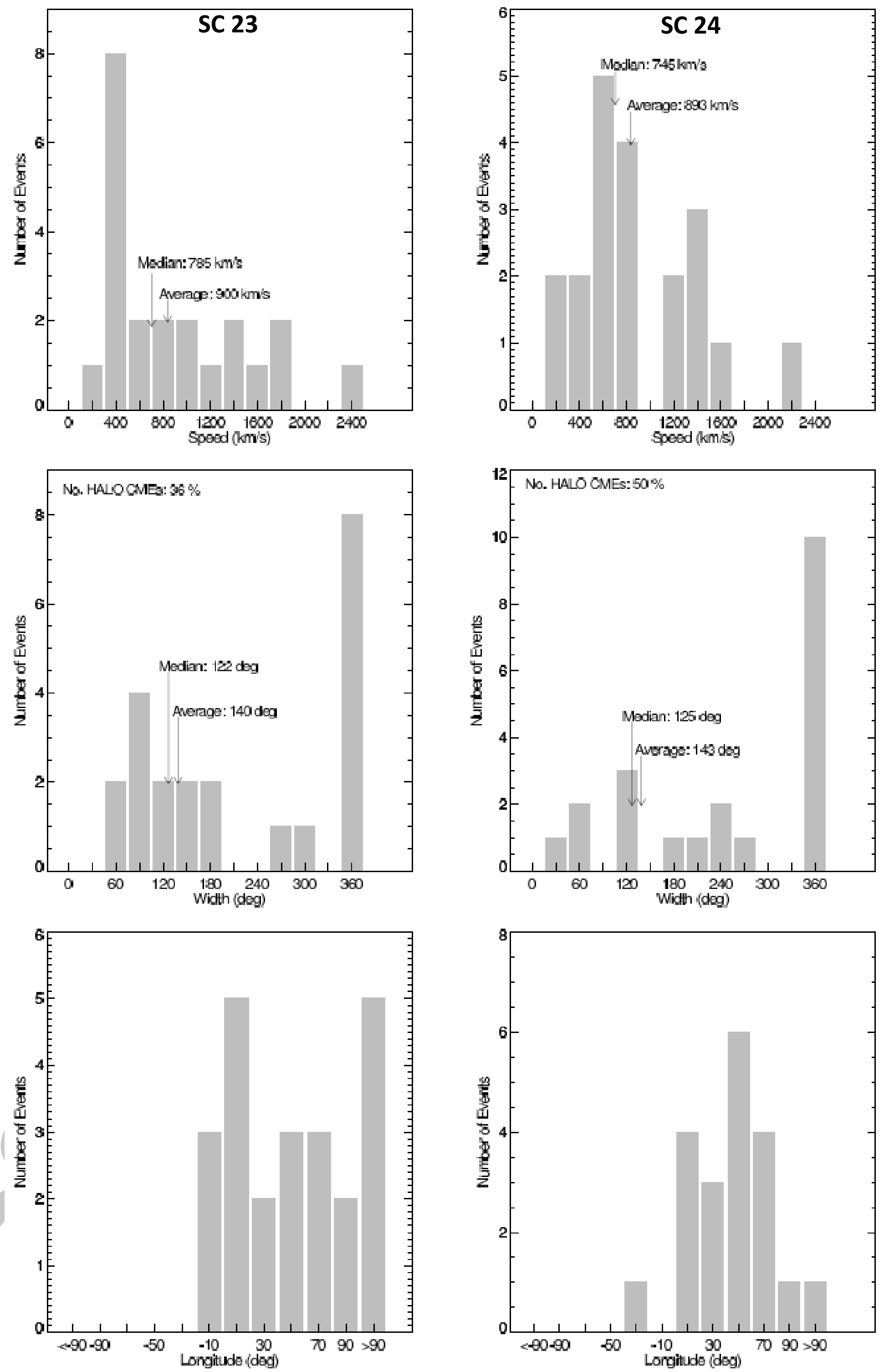

Figure 4: Properties of CMEs associated with SEPs: Speed (top panel), Width (middle panel), and Location of the CME source region (bottom panel), respectively during the rising phase of solar cycle 23 (left) and 24 (right).

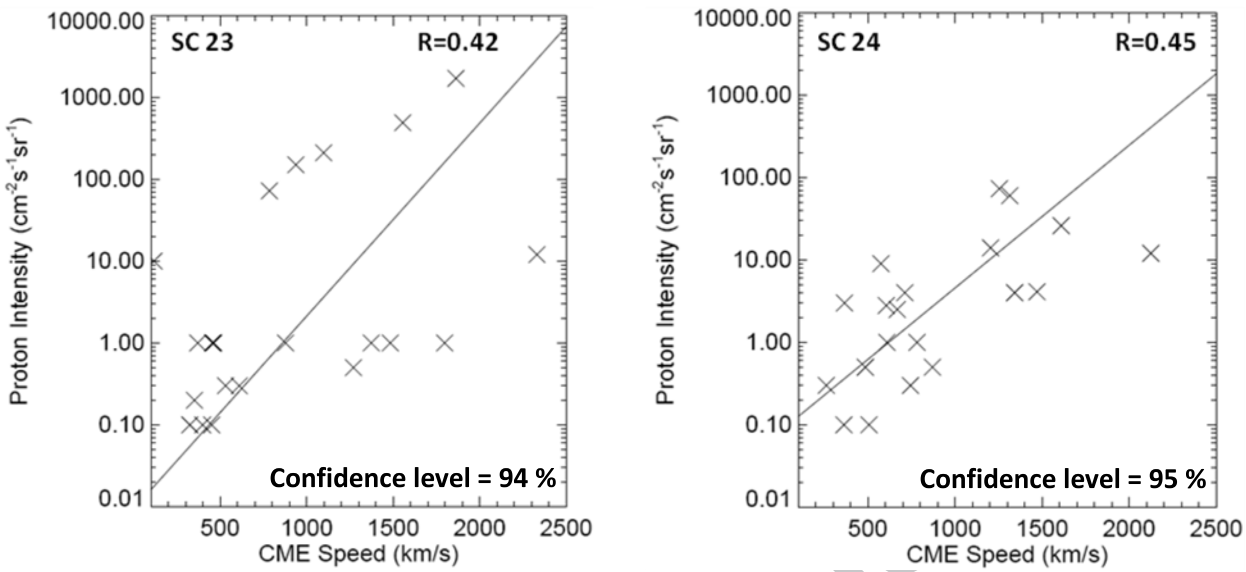

Figure 5: Scatter plots between CME speed and proton intensity for the rise phases of solar cycle 23 (left) and 24 (right). The regression line, correlation coefficients (R), and confidence level are also shown in the figure.

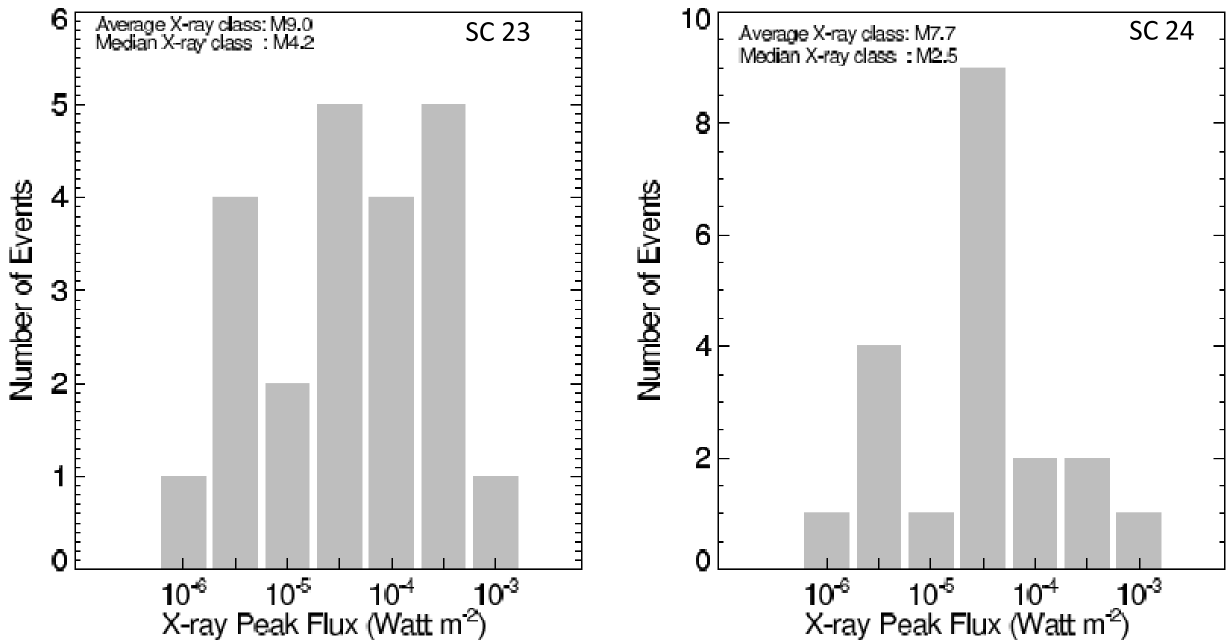

Figure 6: Distribution of GOES X-ray peak fluxes during the rise phase of solar cycle 23 (left) and 24 (right). The average and mean flare sizes are also indicated on the plots.

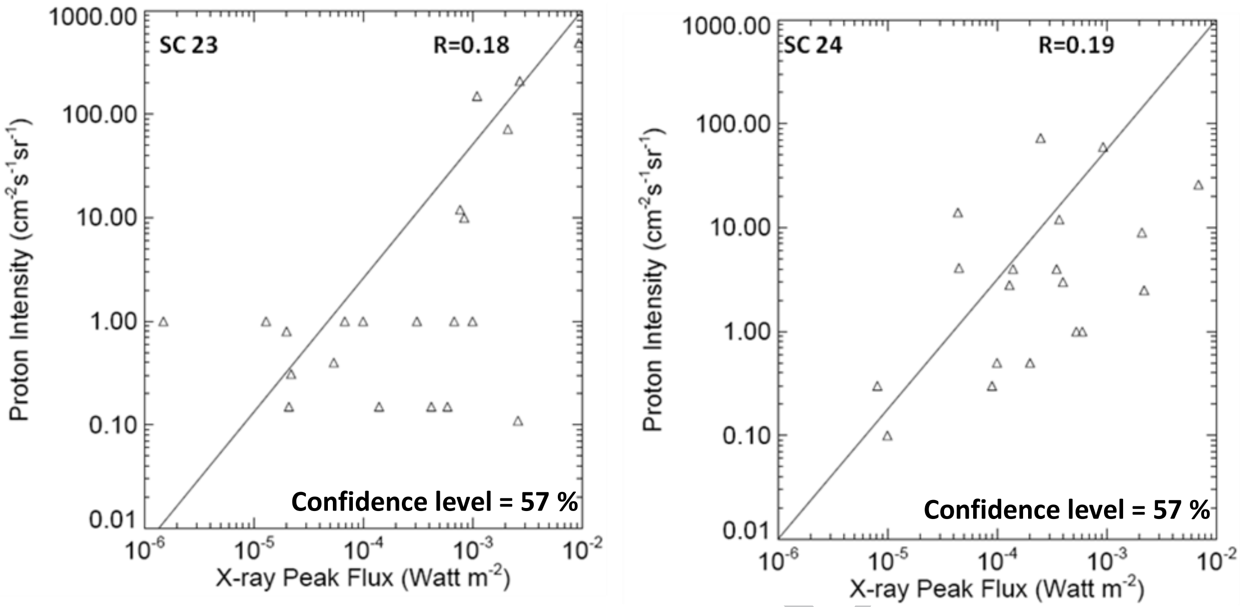

Figure 7: Scatter plots between X-ray peak flux and proton intensity for the rise phase of solar cycle 23 (left) and 24 (right). The regression line is also shown for each group. The regression line, correlation coefficients (R), and confidence level are also shown in the figure.

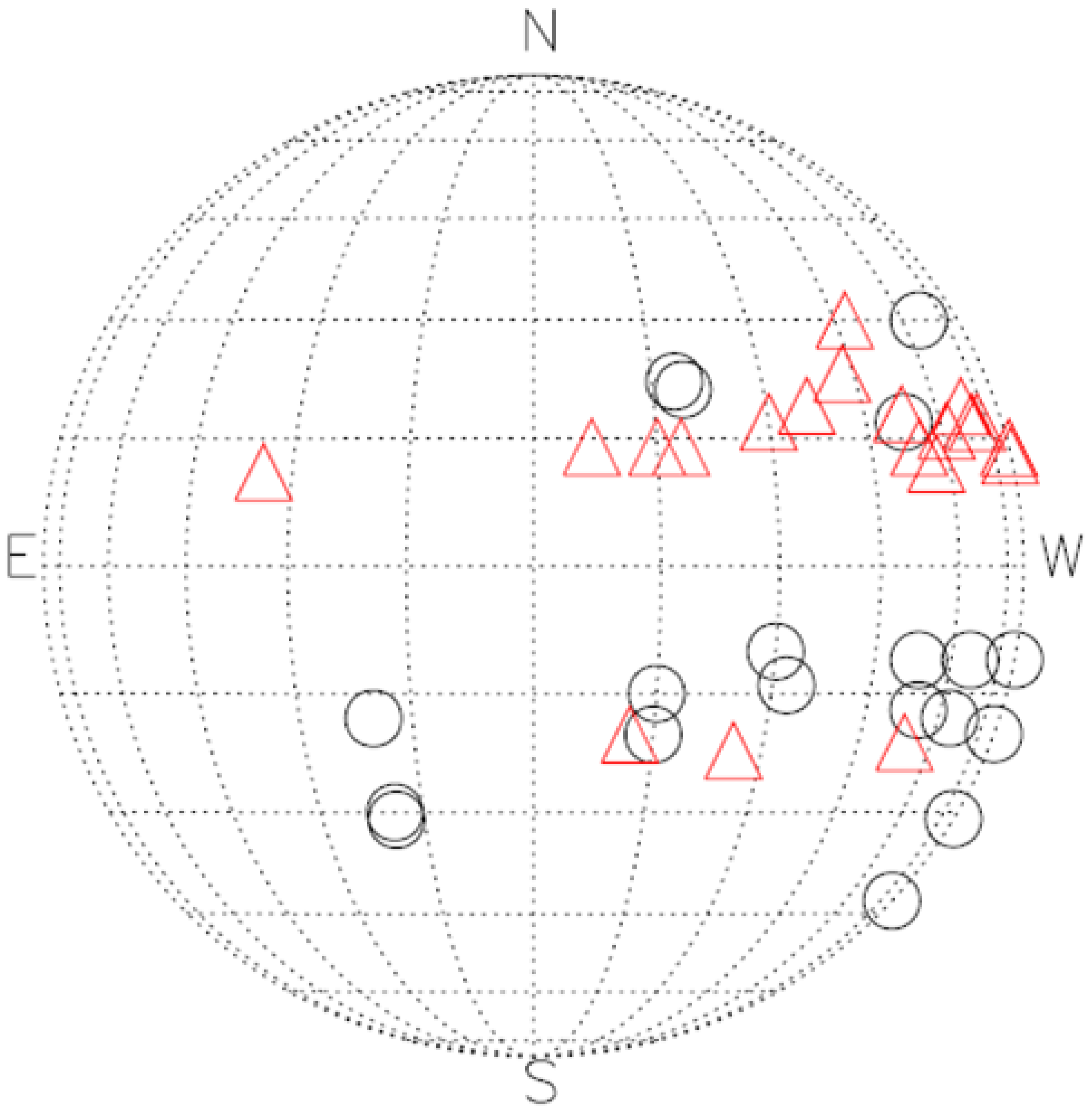

Figure 8: Distribution of SEP source regions on the Sun during the rise phases of solar cycle 23 (black circle) and 24 (red triangle).